The image slicer for the Subaru Telescope High Dispersion Spectrograph

Akito Tajitsu

The Subaru Telescope, National Astronomical Observatory of Japan, 650 North A'ohoku Pl., Hilo, HI 96720, USA

tajitsu@subaru.naoj.org

Wako Aoki

National Astronomical Observatory of Japan, 2-21-1 Osawa, Mitaka, Tokyo, 181-8588

aoki.wako@nao.ac.jp

and

Tomoyasu Yamamuro

OptCraft, 3-16-8-101 Higashi-Hashimoto, Midori-ku, Sagamihara, Kanagawa, 252-0144

yamamuro@optcraft.com

Abstract

We report on the design, manufacturing, and performance of the image slicer for the High Dispersion Spectrograph (HDS) on the Subaru Telescope. This instrument is a Bowen-Walraven type image slicer providing five 0.3 arcsec × 1.5 arcsec images with a resolving power of $R = \lambda/\delta\lambda = 110,000$. The resulting resolving power and line profiles are investigated in detail, including estimates of the defocusing effect on the resolving power. The throughput in the wavelength range from 400 to 700 nm is higher than 80%, thereby improving the efficiency of the spectrograph by a factor of 1.8 for 0.7 arcsec seeing.

1. Introduction

Optical spectroscopy with a very high resolving power ($R = \lambda/\delta\lambda > 100,000$) enables measurements of isotopic abundance ratios including ^{7}Li/^{6}Li, ^{25}Mg/^{24}Mg, ^{151}Eu/^{153}Eu for stellar atmospheres and/or interstellar matter based on detailed analyses of spectral line profiles (e.g., Smith et al. 1993; Kawanomoto et al. 2009; Aoki et al. 2003). These studies also require very high signal-to-noise ratios in general, which can be achieved by large telescopes.

One difficulty in such observations and instrumentation is that the size of the stellar

image at the focal plane increases with telescope aperture, thereby requiring a larger spectrograph with a wider slit width to achieve the same spectral resolution. One solution to achieve very high resolution with high efficiency is to install an image slicer. A brief history of the development of image slicers since Bowen (1938), as well as the application to the VLT/UVES, is provided by Dekker et al. (2003).

The High Dispersion Spectrograph (HDS: Noguchi et al. 2002) on the Subaru Telescope can achieve a very high resolving power, up to 150,000, by applying a very narrow slit. When a slit of 0.3 arcsec (150 μm) width is applied, the resolving power is 115,000. The throughput at the slit is, however, as low as 45 % for the typical seeing size of the telescope at Mauna Kea in Hawaii ($\sim$ 0.6 arcsec). In order to improve the efficiency of the spectrograph for observations with very high resolution, we installed a Bowen-Walraven type image slicer. This type of image slicer traps incident light in a thin plate by total internal reflection, and slices the image by sending the light at every second reflection to a glass prism inclined with an appropriate angle (see figure 1). After the designing of the instrument in late 2008, the instrument was constructed in 2009 and was installed in 2010. The instrument was opened for common-use of HDS from August 2011.

This paper reports on the design and manufacturing of the image slicer for the HDS (§ 2), and its performance as verified using calibration sources and stellar light (§ 3). In particular, the line profiles and spectral resolution obtained with the image slicer are investigated in detail, and the effect of defocusing at each sliced image is discussed. The operation and data reduction procedure are also presented (§ 4).

2. Design and construction

2.1. Optical design

The Bowen-Walraven type image slicer we installed is optimized for the following two prime requirements. The first requirement is to maximize the energy from point sources under the typical seeing of 0.6 arcsec on Mauna Kea. Therefore, the clear aperture should be up to 1.5 arcsec (corresponding to 0.75 mm on the focal plane of the Subaru Telescope). The second requirement is the spectral resolving power as high as $R \sim 110,000$. Therefore, the width of the sliced images should be 0.3 arcsec (0.15 mm). In order to satisfy these two requirements, the image slicer is designed to transform a 1.5 arcsec $\times$ 1.5 arcsec field of view into five sliced images of 0.3 arcsec width as shown in figure 1. In this paper, the five sliced images (hereafter "slices") are numbered 1-5 along the optical path as shown in the figure. The specification of the image slicer is given in table 1. We note that since targets of this instrument are assumed to be bright stars, no slice is dedicated to obtain a background sky spectrum.

Echelle spectra for the slit length of 7.8 arcsec (five 1.5 arcsec images with small separations) are obtained without any overlap between the adjacent orders for wavelengths longer

than 4900 Å (4000 Å) using the red (blue) cross disperser grating. For instance, the wavelength range from 4900 Å to 7600 Å is covered by a single exposure.

A photograph of the optical element of the image slicer is shown in figure 2. The image slicer is made by optical contact of three fused-silica pieces, which are a small triangular prism, a parallel plate, and a large triangular prism with an inclined slicer edge. The reflection losses of the entrance and exit surfaces are suppressed less than 1 % in the wavelength range of 400 - 700 nm by using multilayer anti-reflection coating.

2.2. Layout

The holder of the optical element is designed to mount it in front of the HDS slit without updating of the HDS system for keeping operation with the normal slit. Instead of the normal slit mirror, a pinhole mirror is placed just in front of the image slicer for target acquisition and guiding with the HDS slit viewer. The pinhole diameter is 2.8 arcsec (1.4 mm) and the location is 6.97 mm from the typical slicer edge position. This makes a 1.7 arcsec (0.83 mm) clear image without vignetting in the image slicer, and also makes a blurred region around the clear image. The blurred region, corresponding in general to outer region of a target star, produces a weak envelope on one-side of the first slice, resulting in a small decrease of the spectral resolution as described in § 3.2. Just behind the image slicer, a 8.8 arcsec (4.4 mm) × 1.2 arcsec (0.6 mm) rectangular mask is placed to suppress scattered light. After the mask, the sliced images pass through the HDS slit that is fully opened for working not as a slit but as an open aperture. The sliced images are then aligned just on the center of the HDS slit position by a mechanism connected with the holder that adjusts the x-shift, y-shit, and position angle. In the holder, the slicer edge is located 6.32 - 8.51 mm from the HDS slit, and the HDS collimator is shifted to focus on the image slicer instead of the normal slit (see next section).

The above layout is different from that of the image slicer for the VLT/UVES (Dekker et al. 2003). The UVES image slicer is mounted just on the VLT focus, and sliced images are re-focused on the UVES slit by a relay optical system. This layout makes up a sharp slit image by the normal slit even for the sliced images, avoiding degradation of spectral resolution by defocusing effect. On the other hand, our layout avoids light loss due to vignetting by a slit and reflection at relay lens surfaces. In addition, our layout simply enables us to add the image slicer without updating of the HDS slit and the slit viewer mechanism.

3. Performance of the instrument

3.1. Instrument setup

As shown in figure 1, the individual sliced images are located 6.32–8.51 mm from the HDS slit. These offsets are (partially) compensated by the shift of the collimator position. In order to find the correct position of the collimator, we first focused the camera system using the normal slit (Noguchi et al. 2002). Then, we searched for the collimator position that produces
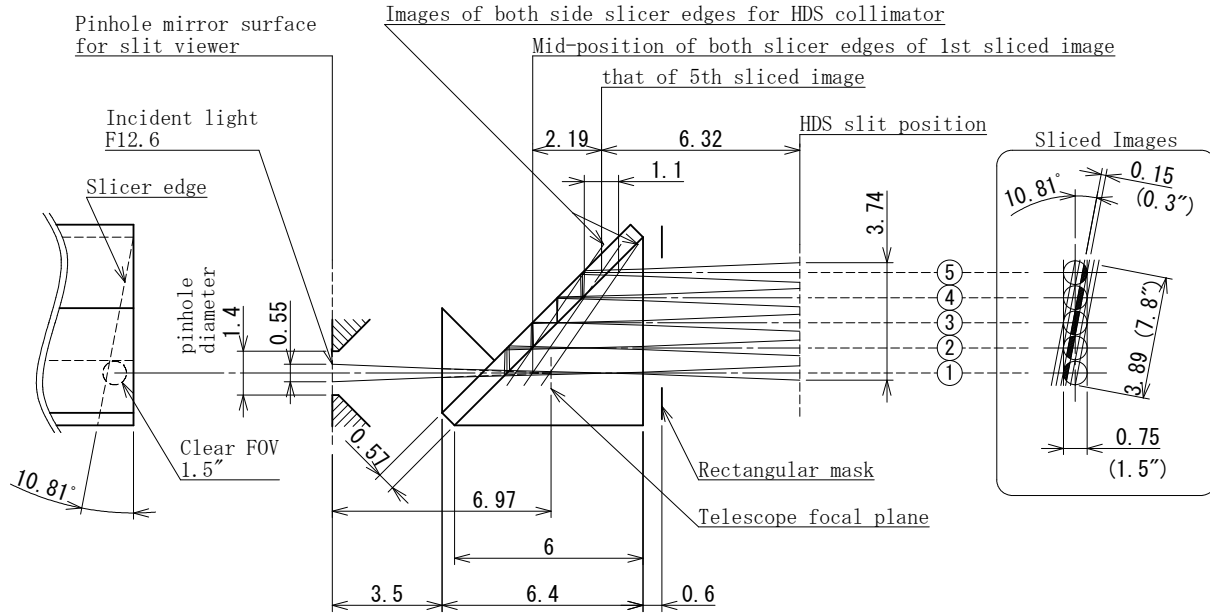
Fig. 1. Optical design of the image slicer. The light from the telescope enters from left through the pinhole that is sufficiently large to make a clear field-of-view of 1.5 arcsec required for observations (the clear field of view is actually 1.7 arcsec). The light is reflected in the thin (0.57 mm) plate and escapes to the inclined prism (by 10.81 degree) glued to the plate. The right panel shows the sliced images obtained by this instrument.
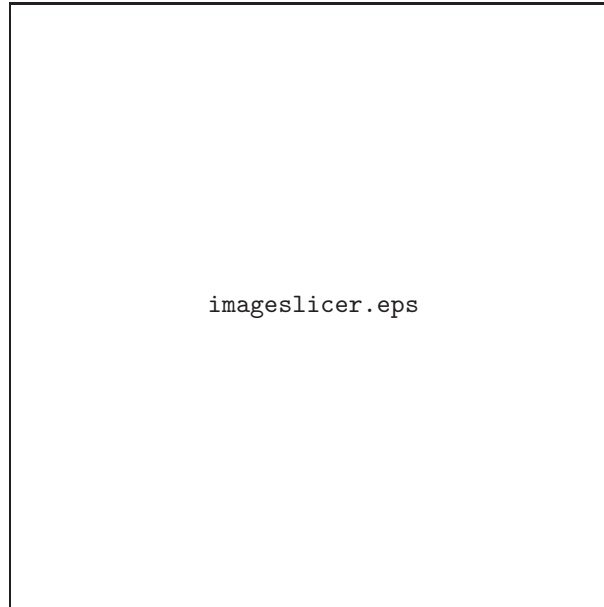

Fig. 2. Photograph of the optical element of the image slicer

4

Table 1. Specifications of the image slicer

Type	Bowen-Walraven type
Number of slices	5
Entrance	1.5 arcsec × 1.5 arcsec
Sliced image	0.3 arcsec × 7.8 arcsec
Wavelength coverage	400–700 nm
Plate thickness	0.57 mm
Material	fused-silica

the highest spectral resolution with the image slicer. This results in a shift of the collimator by 7.3 mm. This well agrees with the expectation from the design of the mount holder for the third-fourth slices.

The differences of the best focus positions for individual slices result in degradation of spectral resolution. This problem is discussed in the next subsection.

The spectral format (spectral images on the detector) obtained with the image slicer is set to be the same as that obtained with the normal slit by applying a small offset to the cross disperser grating angle. As a result, direct comparisons of spectral images obtained with and without the image slicer are possible. Figure 3 shows stellar spectral images (o Per) obtained with the image slicer and a normal slit with a 0.3 arcsec width. In the central spectrum of each panel, absorption features of telluric lines appear. Figure 4 shows a cross cut of the CCD image for a spectrum obtained with the slicer, in which five slices are identified corresponding to those presented in figure 1. The cross cut for a spectral image of the flat lamp is also depicted for comparison purposes by the thin line.

3.2. Spectral resolution and line profile

The spectral line profiles and the resolving power are measured for weak emission lines of Th-Ar arc spectra. Figure 5 shows a section of the CCD image obtained with and without the image slicer. The image without the slicer is obtained with the slit of 0.3 arcsec (0.15 mm) width and 7.5 arcsec (3.75 mm) length.

Figure 6 shows the spectral profiles of ten weak Th emission lines around 670 nm with different symbols for individual lines, which are normalized at the peak by fitting gaussian profiles. The solid line is the gaussian profile for the average of the full width half maximums measured from the individual lines. The measurements are made for the five slices. The Th-Ar spectrum obtained with the normal slit is also separated into five spectra using the same sub-apertures as for the extraction of spectra obtained with the slicer.

The line profile of the central (the third) slice is shown in the figure as an example. There is apparently no clear difference between the resolution and the profile between the spectra with and without the image slicer. The average of the spectral resolution, $R = \lambda/\delta\lambda$, where $\delta\lambda$ is
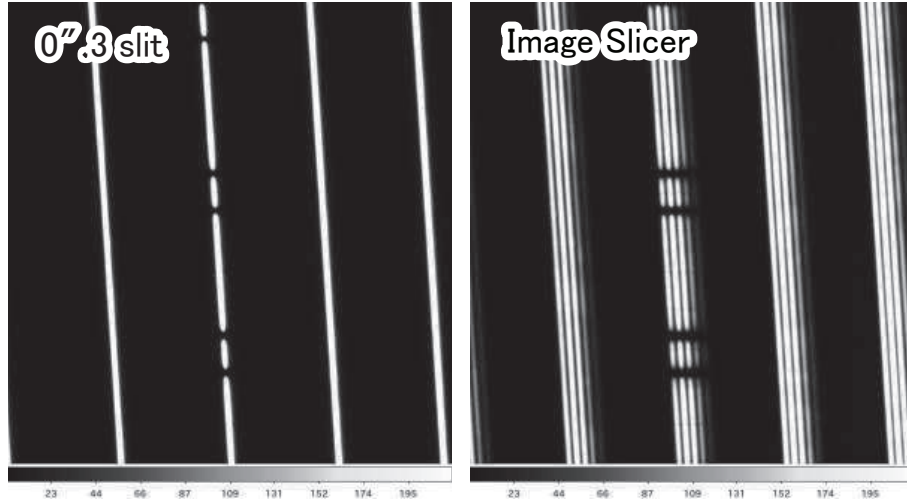
5

Fig. 3. The CCD image of a stellar spectrum (o Per) obtained with the image slicer (right) and that with the normal slit with 0.3 arcsec width (left).

determined as the FWHM of the profiles for individual lines, is typically 110,000 when the image slicer is used. For comparisons, the resolution is 114,000 when using a 0.3 arcsec slit without the image slicer (see below for more details).

Similar results are obtained for other slices. The exception is the first spectrum that appears in the right edge of the spectral image in figure 5. The profile of the spectrum of this slice (figure 7) shows some asymmetry and lower spectral resolution ($R \sim 90,000$). This is due to the contribution of the blurred light around the clear image formed through the pinhole on the first slice (§ 2.2).

The spectral resolution obtained at each slice is shown in figure 8. The resolution obtained with the 0.3 arcsec slit is approximately 114,000. The reason for the weak dependence of the resolution on the position at the slit is unclear.

The spectral resolution obtained with the image slicer is highest at the fourth slice, suggesting that the collimator focuses around this position (see also § 3.1). The resolution decreases by about one percent at the adjacent slices, and by four percent at the second slice. The resolution at the first slice is significantly lower for the reasons mentioned above.

3.3. Throughput

The throughput of the image slicer is measured using the calibration lamp for flat-fielding. The flat lamp is stable at the 0.1 % level (Tajitsu et al. 2010). The photon counts of the flat data obtained with the image slicer are normalized by those obtained without the slicer. Figure 9 shows the result as a function of wavelength. The measurements are made for three different setups with different wavelength coverages. The count is measured at the center of the spectral image for each echelle order.

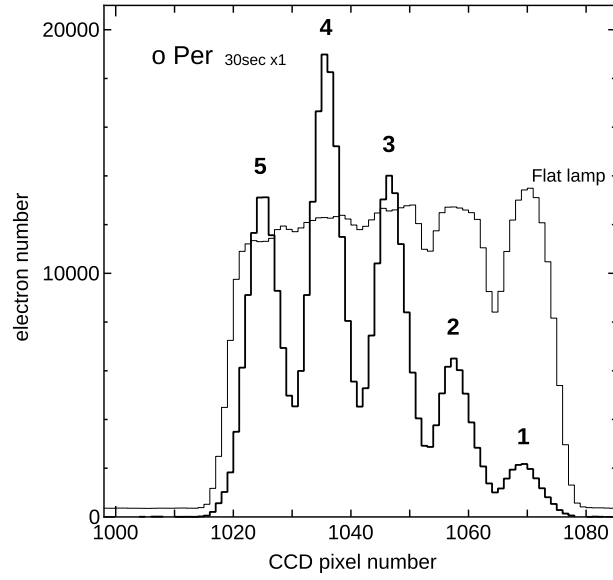The throughput of the image slicer is 80–85 % in the wavelength range from 400 nm

6

Fig. 4. A cross cut image of the spectral data for an object (o Per) and the flat lamp obtained with the image slicer. The low counts between the first and second slices found in the flat lamp data are because the beam from the flat lamp passes through the pin hole, which is in front of the image slicer, and the first slice is not fully illuminated (see Figure 1).
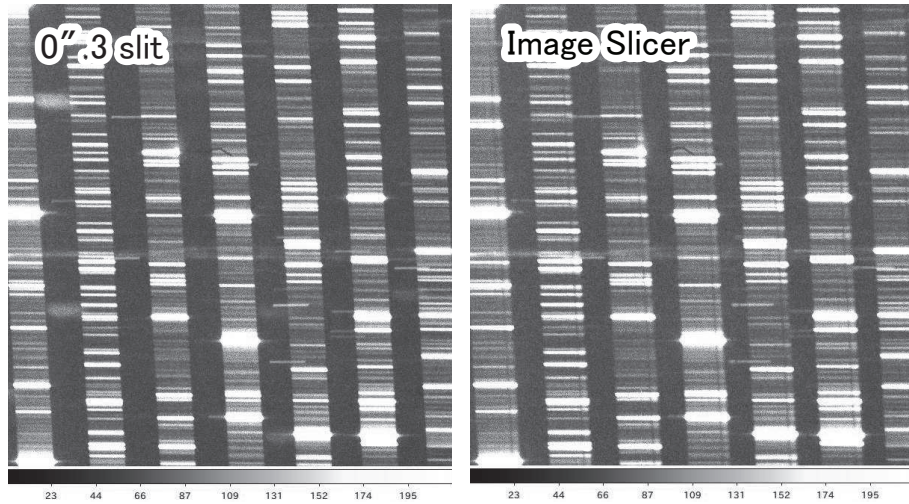

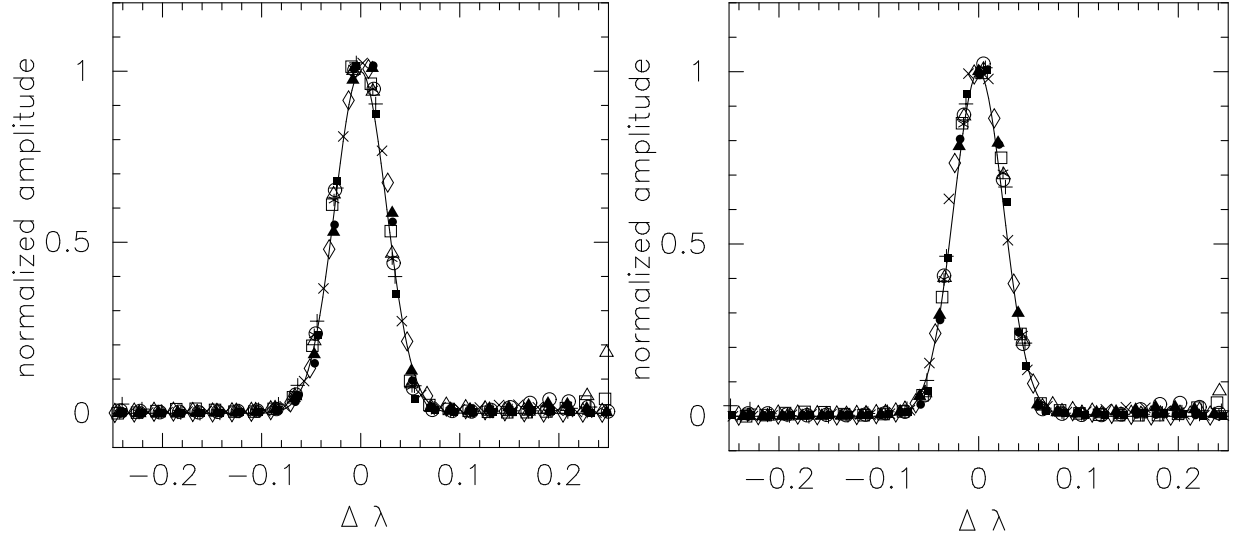**Fig. 5.** The same as figure 3, but for Th-Ar spectra.

Fig. 6. Line profiles of 10 Th lines around 670 nm obtained with the third (central) slice (left) and that of the center of the slit without the slicer (right). Individual lines are normalized at the peak by gaussian fitting and shown by data points with different symbols. The solid line indicates the gaussian profile for the average of the full width half maximums measured for individual lines. There are no significant differences in the width and profile between the two spectra.
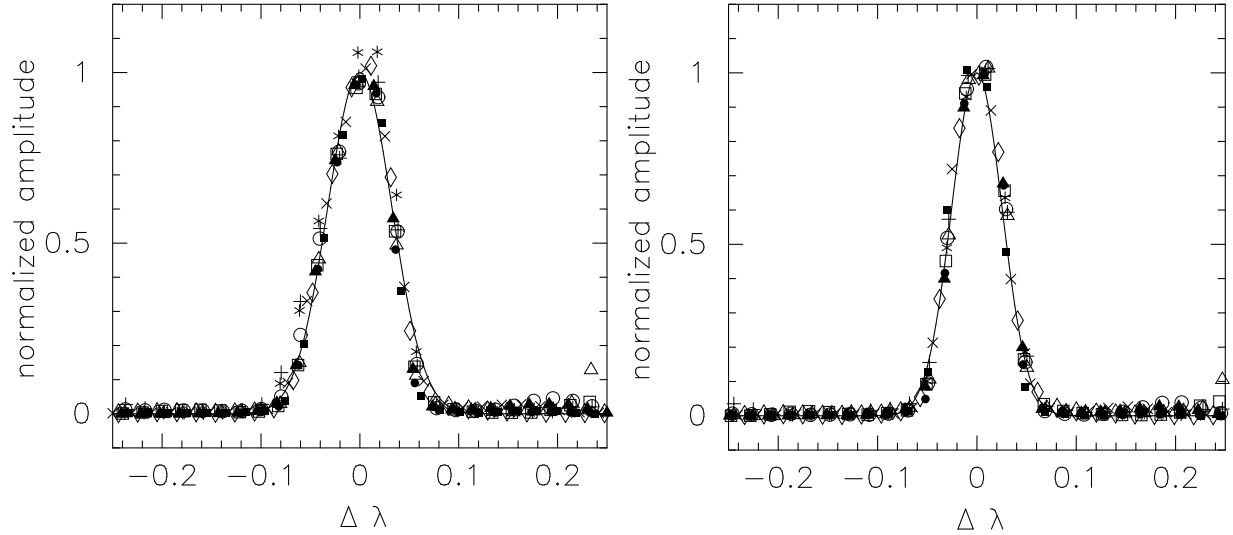

Fig. 7. The same as figure 6, but for the first slice (left) and the corresponding data without the slicer (right). The spectral line of this slice is wider and shows some asymmetry.
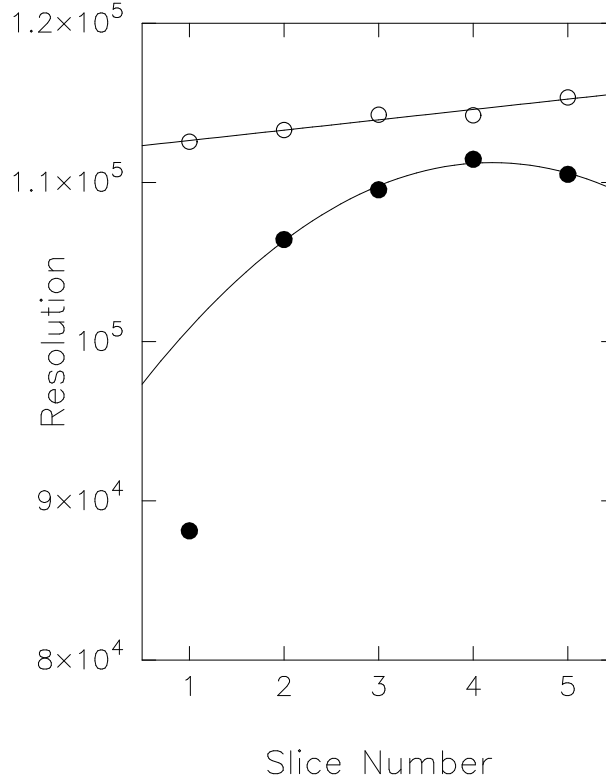
8

Fig. 8. The spectral resolution of each slice (number 1-5) obtained with the image slicer (filled circles) and with the slit of 0.3 arcsec width (open circles). The parabola and linear fits are made for these data points. The first slice is excluded in the fit for the data obtained with the image slicer (see text).

to 700 nm, to which the AR coatings on the planes of incidence and injection are optimized. The loss by the reflection at the two surfaces of the slicer is expected to be as low as 1 % in the above wavelength range. The loss of light through the reflections inside the slicer due to the absorption and/or scatter by small particles would be as large as 10 %. This can be estimated from the decrease of the flat light from the first to fifth slices (see figure 4). Another potential source of loss is the scatter at the slicer edges. Though the scatter is expected to be smaller than 5 % from the manufacturing errors of the edges ($< 10 \ \mu$m), the estimate could be uncertain. The total throughput expected from the above estimate is 85–90 %. Although the measured throughput is slightly lower than this estimate, the instrument significantly improves the efficiency of the observations (see § 4.3).

3.4. *Comparison of stellar spectra obtained with and without the image slicer*

We obtained spectra of bright stars to compare the spectra obtained using the image slicer with those obtained with the 0.3 arcsec slit. Figure 10 shows the spectra of o Per observed with the S/N ratios of 530 (with the image slicer) and 400 (without the image slicer) at 6860 Å. The seeing when the both spectra were taken was 0.68 arcsec. The spectra obtained from the five individual slices were combined. Many sharp absorption lines of O_2 molecules
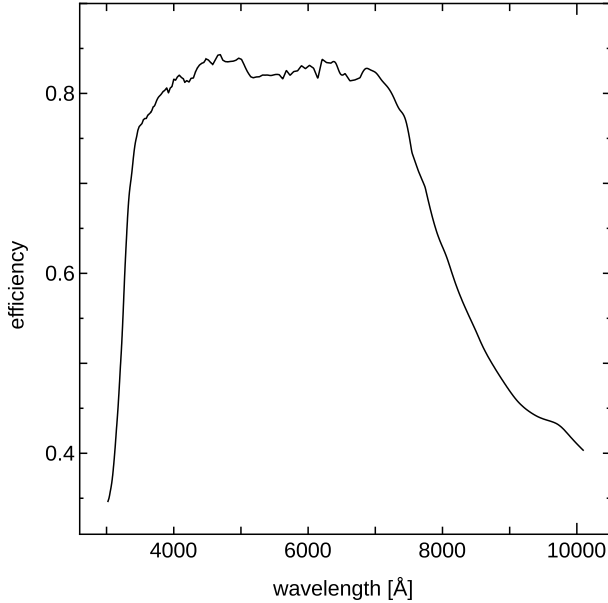
9

Fig. 9. Throughput of the image slicer as a function of wavelength measured with the calibration lamp for flat-fielding.

in the Earth's atmosphere appear in this wavelength range. We note that the continuum normalization is uncertain in the range where many absorption lines are overlapping. However, the same normalization procedure with the IRAF task "continuum" is applied to both spectra with and without the image slicer, which basically cancel the uncertainty in the comparison of the two spectra.

As expected from the comparisons of the Th-Ar emission lines (§ 3.2), no significant difference is found between the two spectra. We note that the spectrum obtained from the first slice, whose line profile is not as sharp as in other spectra (§ 3.2) is included in the stellar spectrum. However, since the contribution of the first slice to the final data is less than 5 % (figure 4), the effect is negligible in the comparison. However, in the event of poor seeing, in which the fraction of light in the first slice is non-negligible, the light from this slice may be ignored if high spectral resolution is paramount.

4. Telescope setup, operations and data reduction

4.1. Target acquisition and guiding

The target acquisition is made using slit viewer images. The slit viewer camera for the HDS is applied with no modification to the image reflected by the plane mirror in front of the slicer. The target is centered on the pinhole opened on the mirror that introduces the stellar light to the image slicer (figure 11). Since the plane mirror is 6.97 mm in front of the slicer on which the telescope should focus during observations, off-focus images are acquired with the slit viewer camera for guiding. However, the resulting image size of about 1.0–1.5 arcsec is
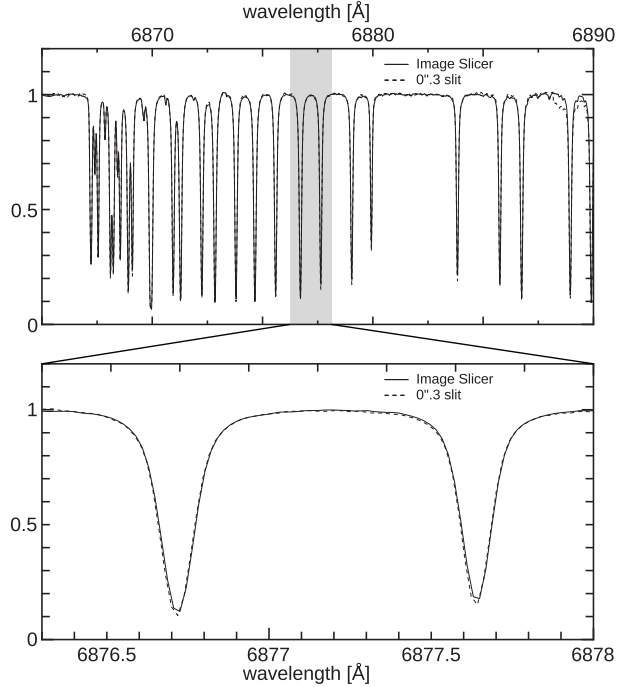
10

Fig. 10. Comparison of stellar spectra obtained with and without the image slicer shown by the solid and dashed lines.

sufficient to guide the target to the pinhole, because targets of this instrument observed with very high resolution are assumed to be bright objects.

4.2. Telescope focusing

Since the position of the image slicer is different from that of the original HDS slit, some offset of the telescope focus position is necessary and this is achived by shifting the secondary mirror. There is no facility to directly measure the image size at the position of the slicer. Hence, the telescope focusing is performed using the slit viewer images. The secondary mirror is then positioned with an offset that was empirically determined to maximize the photon counts at the central (third) slice.

4.3. Advantages of the image slicer

An example of comparisons of spectra obtained with and without the slicer for the same exposure time is shown in figure 12. The observation was taken in 0.68 arcsec seeing. The photon counts of the spectrum obtained with the slicer are approximately 1.8 times higher than that obtained with the normal slit.

Figure 13 shows estimates of the fraction of light that enters the spectrograph through the slit or the image slicer as a function of the seeing size. The dotted line indicates the value for the 0.3 arcsec slit, while the solid line shows the same for the image slicer.

The gain of photons expected by using the image slicer, that is, the ratio of the fraction
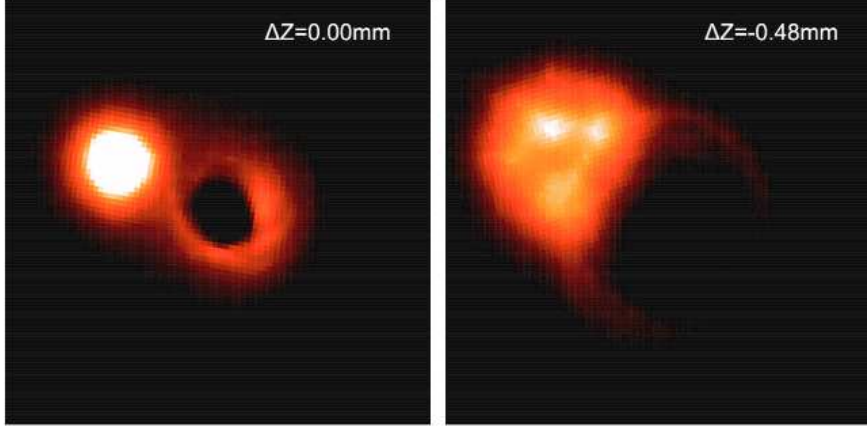
11

Fig. 11. Slit viewer images for target acquisition and guiding. The left is the image obtained by focusing the telescope on the pinhole mirror in front of the image slicer. The target (ρ Oph) is on the pinhole of a 2.8 arcsec diameter at the mirror (center of the image). The companion star, 3 arcsec away from ρ Oph, also appears in this image. The right is the image after focusing the telescope on the image slicer. The guiding is made for such off-focus images. As seen in this image, objects around the target within several arcsec could result in contamination.

of light entering to the spectrograph with the image slicer to that for the 0.3 arcsec slit, is higher than unity for the seeing size larger than 0.3 arcsec, and reaches to two at 0.8 arcsec. This is confirmed by observations for some cases, as shown in figure 12. Hence, to obtain spectra with the resolution as high as $R = 110,000$, a higher S/N is expected by using the image slicer in any usual seeing condition at Mauna Kea.

On the other hand, the spectrum with the image slicer spreads over much number of CCD pixels along the slit length direction. The resultant spectrum is affected by the increase of the dark current, the readout noise and the sky background. Moreover, the telescope guiding and the target acquisition by the off-focus image (section 4.1) of faint targets could be difficult during actual observations. Given these disadvantages for faint targets, the image slicer is useful for objects brighter than 15 magnitudes.

4.4.   Data reduction technique

In order to obtain the best quality data, the spectra should be extracted separately for the five slices, for which wavelength calibration is made using comparison Th-Ar spectra obtained by the same procedure for the object data. Special care is required at the edge of the flat image (left- and right-hand sides of the fifth and first slices of the flat data: see figure 4), because the regions of the detector illuminated by the flat lamp are sometimes smaller than for those of an object.

The best quality spectrum is obtained by combining the four spectra of 2-5th slices after wavelength calibration. However, the resolving power of $R \sim 110,000$ is well achieved by combining the four spectra before wavelength calibration, which significantly reduces the
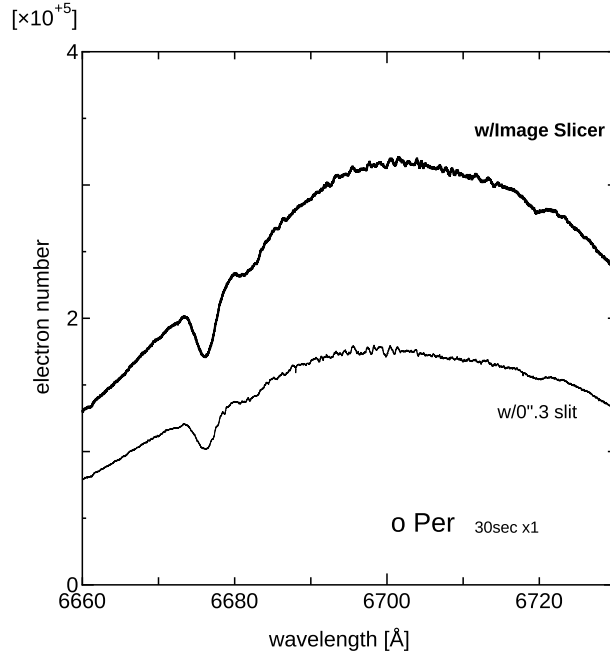
Fig. 12. A comparison of spectra of o Per obtained with and without the image slicer. Each spectrum is flat-fielded and wavelength-calibrated, but is not normalized. The photon counts obtained with the slicer are 1.8 times higher than those with normal slit with the same exposure time, under the 0.68 arcsec seeing condition.
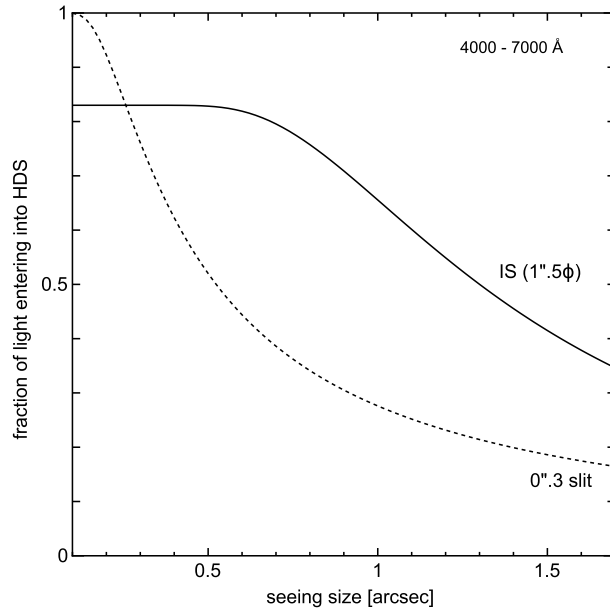

Fig. 13. Fraction of light that enters into the spectrograph through the 0.3 arcsec slit (dotted line) and that through the image slicer (solid line)

13

reduction procedure. The first slice might be used to increase the photon counts, but that could result in a small decrease of spectral resolution.

5. Summary

The design, manufacturing, and performance of the image slicer for the Subaru/HDS are reported. Such an instrument enables one to obtain very high resolution spectra with high efficiency. The instrument is already available for the common-use of HDS. A similar instrument is also installed in the spectrograph of the 1.88 m telescope at Okayama Astrophysical Observatory (OAO/HIDES: Izumiura et al. 1999), which contributes to increasing the efficiency of the observations with high resolving powers.

The image slicer reported here is designed to obtain a very high resolving power ($R \sim$ 110,000). We are also planning to install another image slicer that provides smaller number of wider slice images (e.g. three slices of 0.5 arcsec) to increase the efficiency of observations with more usual spectral resolution ($R \sim 80,000$). The new image slicer will be installed in mid-2012 and also be opened for common-use. Such efficient image slicers will be more useful for next generations of larger telescopes.

References

Aoki, W., et al. 2003, ApJL, 592, L67

Bowen, I. S. 1938, ApJ, 88, 113

Dekker, H., Nissen, P. E., Kaufer, A., Primas, F., D'Odorico, S., & Hanuschik, R. W. 2003, Proc. SPIE, 4842, 139

Izumiura, H. 1999, Observational Astrophysics in Asia and its Future, 77

Kawanomoto, S., et al. 2009, ApJ, 701, 1506

McWilliam, A., & Lambert, D. L. 1988, MNRAS, 230, 573

Noguchi, K., et al. 2002, PASJ, 54, 855

Smith, V. V., Lambert, D. L., & Nissen, P. E. 1993, ApJ, 408, 262

Tajitsu, A., Aoki, W., Kawanomoto, S., & Narita, N. 2010, Publ. Natl. Astron. Obs. Japan, 13., 1 (http://library.nao.ac.jp/naopublication/)